Field emission vacuum power switch using vertically aligned carbon nanotubes

N. L. Rupesinghe,[a] M. Chhowalla, K. B. K. Teo, and G. A. J. Amaratunga
Department of Engineering, University of Cambridge, Trumpington Street, Cambridge CB2 1PZ, United Kingdom

(Received 3 April 2002; accepted 1 July 2002; published 3 February 2003)

A field emission vacuum switch using vertically aligned carbon nanotubes grown by a direct current plasma enhanced chemical vapor deposition is reported. Cathodes with optimized field emission properties were evaluated in diode configuration as a test vehicle for the construction of a vacuum power three terminal triode device. Limiting factors such as space charge effects involved with high current densities (more than 10 mA/cm^2) are also investigated using computer simulations. © *2003 American Vacuum Society.* [DOI: 10.1116/1.1527635]

I. INTRODUCTION

Recently well-aligned carbon nanotubes have been explored for field emission (FE), electrochemistry and energy storage applications.[1–6] There is great potential for a field emission cathode, which could deliver high currents (more than 10 mA) in applications such as vacuum power switches and microwave tubes.[7–11] At large emission currents factors such as space charge effects within the electron beam, anode material and anode design become important factors, which need careful consideration. A power switch has to be able to block very high voltages in the off state. To be a viable alternative to present day solid state Si devices it must be capable of blocking at least 20 kV, double the maximum voltage rating of a Si device. In addition, the on state voltage across the power switch should be minimal when conducting current in order to minimize the energy loss. The other requirement is fast switching, which is an inherent advantage for a field emission based vacuum device. The anode to cathode gap has to be large enough to block the high off state voltage, which also allows a good vacuum to be maintained. The cathode in a vacuum power switch must be able to deliver high currents at low turn on fields. Field emission (FE) from carbon nanotubes is possible at low applied electric fields due to their high aspect ratio.[12] The maximum amount of FE current reported from one multiwall nanotube is $\sim$0.1 mA, close to the theoretical limit of tube destruction by resistive heating.[13] Dean and Chalamala suggest that an individual SWCNT exhibits current saturation above 100 nA and this current saturation was a direct result of the removal of adsorbates which enhance field emission at high currents.[14] For measurements involving multiple tubes, Collins and Zettl attribute current saturation to interaction of electron beams emitted from neighboring nanotubes.[15] The field emission characteristics of both MWCNTs and SWCNTs have been shown to exhibit Fowler–Nordheim (FN) emission prior to saturation above $\sim 1\ \mu$A.[16] In addition to their remarkable field emission properties, chemical inertness and mechanical robustness make nanotubes promising as cold cathodes for high current applications.

[a]Electronic mail: nlr22@eng.cam.ac.uk

II. EXPERIMENT

The growth process and the material characteristics of the VACNT grown using a direct current plasma enhanced chemical vapor deposition (dc PECVD) system are reported in detail elsewhere.[17] Briefly, the VACNTs are grown at 700 °C onto Ni coated Si or highly polished graphite substrates by initiating a dc glow discharge plasma of C_2H_2 and NH_3 (ratio=75 sccm:200 sccm) at -600 V using an AE 1 kW dc generator. The diode-type field emission measurements were carried out using parallel plate configuration. A $\sim$0.3-μm-thick evaporated metal (high purity Al) film on glass was used as the anode plate. Emission from the sample edges was avoided by always using an anode that was smaller than the cathode. The sample under investigation (cathode) was separated from the anode using high-quality optical grade quartz fiber spacers of known diameter (200 μm). Special care was taken to keep the two fibers 2–3 mm away from the metal section of the anode to avoid any leakage current through the fibers. All measurements were obtained using a Kiethley 237 source measure unit under computer control within a LabView software suite. The field emission properties were optimized by controlling the size, length and the density of the nanotubes (Fig. 1). This was achieved by controlling the growth parameters such as the thickness of the catalyst (Ni or Co) layer, acetylene to ammonia ratio and the deposition temperature.[17] The field emission properties of VACNTs similar to those shown in Fig. 1 are plotted in Fig. 2. Considering the requirements for the power transfer, VACNT cathodes with optimized field emission properties were subjected to further tests. By using a mask, anodes of several sizes were evaporated onto a glass plate such that they could be individually biased to study the current scaling factor with area while keeping other parameters the same. The field emission current as a function of the anode area is plotted in Fig. 3. A schematic of the patterned Al/glass anode is also sketched in the inset of Fig. 3.

A simulation study was carried out using the SILVACO ATLAS[18] device simulation software suite to understand the current limitation mechanisms. Although this software is designed to simulate semiconductor devices, it has been modified to simulate current transport in a vacuum by adapting

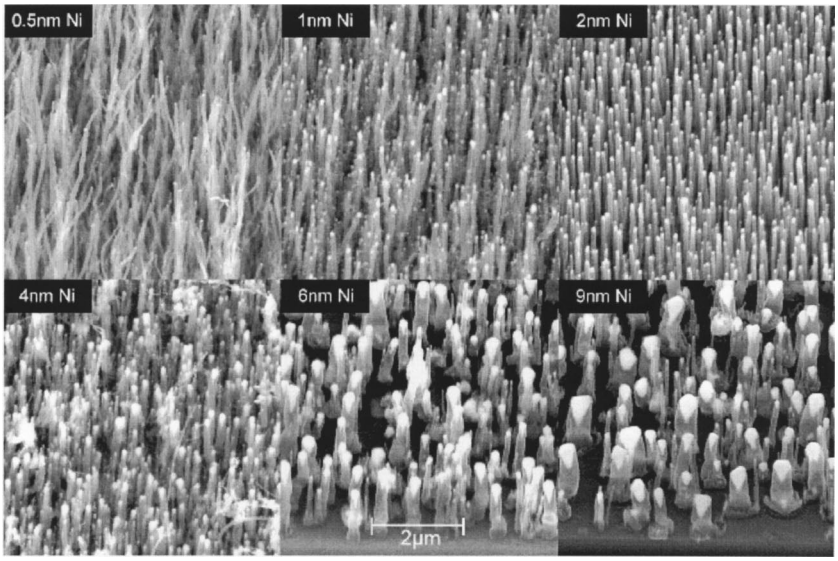

FIG. 1. Nanotubes' growth on varying initial Ni thickness.

the field dependent parameters. First, a material having the same properties as vacuum, zero conductivity and dielectric constant of one, was defined. Then the VACNT structure was constructed with a cathode having a single nanotube of 20 nm diameter and 1 μm high on a metal substrate. Then electron transport properties experienced by electrons in a vacuum were accounted for by calculating the mobility of electrons as a function of potential with respect to the position. Space charge effects in vacuum are accounted for through solution of the computed Poisson-drift equations. All diffusion current was suppressed by defining the simulation temperature to be 0 K. The Fowler–Nordheim equation was used to simulate electron emission into the vacuum via the nanotube. The simulated $I-V$ results from a single nanotube with inter-electrode spacing of 200 μm are shown in Fig. 4.

The triode construction consisted of a cathode of VACNTs with optimized field emission properties (determined from diode measurements) on a highly polished graphite substrate, a Ti extracting grid (2 mm in diameter) with 50 μm square holes separated by 10 μm grid walls (giving a total transparency of 60%) and a highly polished large graphite anode. The VACNTs cathode was patterned into a 1-mm-diam circular area. The extracting grid was separated from the cathode by a 180-μm-thick quartz plate having a 2 mm hole. The cathode grid and cathode–anode spacing were 180 μm and 1 mm, respectively. Triode FE properties were examined by keeping the anode voltage constant (500, 800 and 1100 V) and measuring anode and gate currents as a function of the gate voltage.

III. RESULTS AND DISCUSSION

The nanotubes' growth on varying initial Ni thicknesses shows an increase in the average tube diameter from ~20 nm (0.5 nm Ni film) to ~400 nm (9.0 nm Ni film). Moreover, the average tube height also decreased from ~8

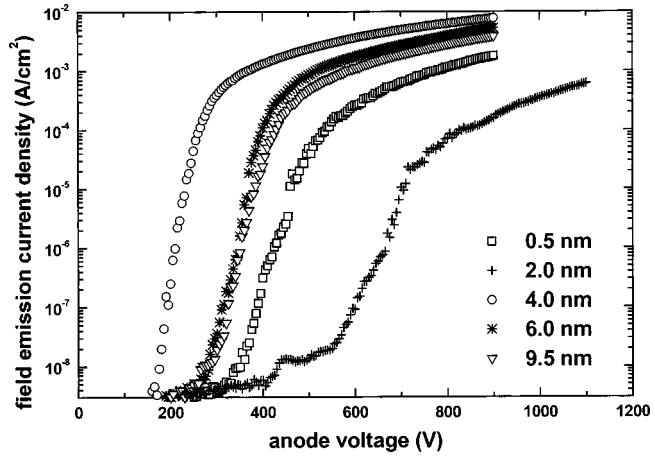

FIG. 2. $J-E$ field emission characteristics measured in diode configuration of the nanotubes in Fig. 1.

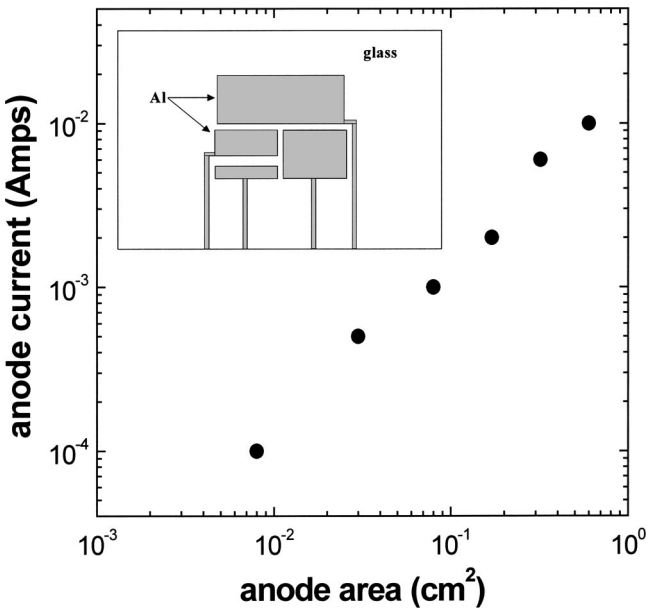

FIG. 3. Actual anode current vs the anode area. A schematic of the Al/glass anode is shown in the inset.

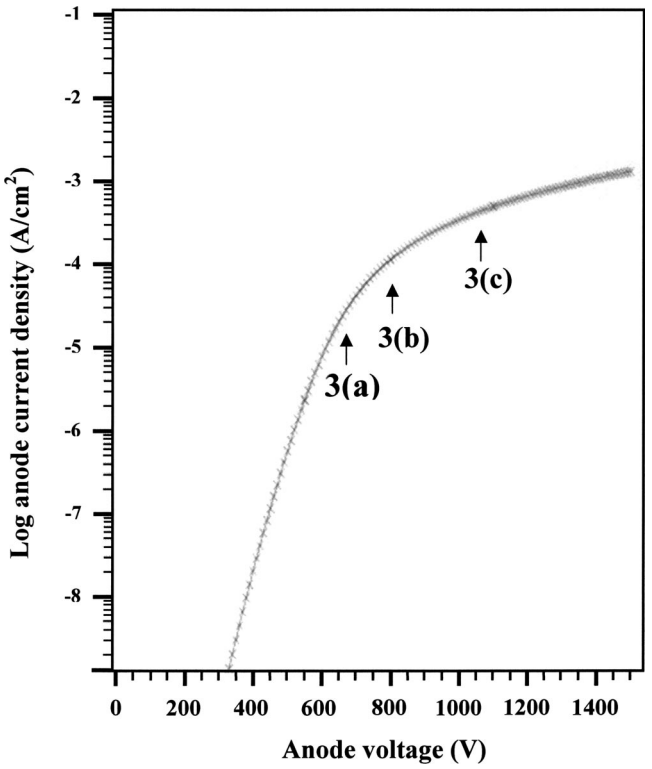

FIG. 4. Simulated $J-V$ characteristics from a single nanotube. The electron concentrations were calculated at points marked (a), (b), and (c) on the curve.

to ~ 3 μm with the increase in Ni film thickness. In addition, the nanotube density decreased from $\sim 10^9$ to 10^8 cm^{-2} with an increase in the Ni film thickness.[17] From the field emission results measured in the diode configuration plotted in Fig. 2, the most uniform and aligned nanotubes grown on 1.9 nm of Ni showed the poorest emission properties with the highest turn on voltage and the lowest saturation current density (0.1 mA/cm^2). This is due to closely packed and uniform height of the nanotubes screening the electric field. Some improvement in emission properties can be seen from the nanotubes grown on 6 and 9.5 nm Ni films with a lower turn on voltage and saturation current density of 5 mA/cm^2. Best field emission properties were seen from short nanotubes grown on an initial Ni film thickness of 4–5 nm, with the lowest turn on voltage and the highest saturation current density ~ 10 mA/cm^2.[19] It can be seen from Fig. 2 that the field emission current does not saturate at the same value and also, since no series resistor was used in the diode circuit, the saturation seen here was not due to any external effect. Additionally, the measured room temperature resistance for these MWCNTs was ~ 3 KΩ[20] and, therefore, too small to limit current at the levels observed in field emission. The field emission current as a function of anode area (Fig. 3) shows a linear variation. This is a clear indication of emission being adequately uniform for scaling to higher currents. From the diode results it is clear that the nanotubes with the best field emission properties also start to show emission current saturation ~ 1 mA/cm^2. At the high current densities measured here, the Al on glass anodes were observed to vaporize. The vaporization of the Al thin film serving as the anode is not surprising when noting that the total power dissipation through the anode is several watts (2–8 W).

Computer simulation of the diode structure was carried out using a single (20-nm-diam, 1 μm height) nanotube placed in the middle of a 60 μm aperture. The simulations were carried in two dimensions. The anode cathode gap was set to 200 μm, the same as that used in our experiments. In order to gain insight into the current saturation phenomena, which apply in a nanotube emitter, the emission from the simulated NT was adjusted by changing the emission barrier in the FN expression to obtain the same current density (J) versus voltage (V) curve as measured in experiment (Fig. 2). An emission barrier of 0.3 eV gave similar current density characteristics as those observed experimentally. Alternatively, it was possible to use a small sub-nm scale feature on the NT tip to enhance the local surface field (tip on a tip) and obtain the same current density with a 5 eV barrier, that of graphite. The former was performed as it did not add the computational overhead by requiring ultrafine mesh points to resolve sub-nm features. The important point to note is that here the simulation is used to study current saturation due to beam phenomena after field emission in the vacuum gap and not the actual emission mechanism. The calculated $J-V$ curve is shown in Fig. 4. The electron beam profile and density were calculated at points labeled as a, b and c in Fig. 4. The electron beam profile and concentration from the calculated $J-V$ positions marked in Fig. 4 are plotted in Fig. 5. The electron beam profile is presented graphically in Figs. 5(a), 5(c), and 5(e) with the gray scale indicating the electron path along the vertical towards the anode. The actual number of electrons along the anode plane, $y=0$ μm, are plotted in Figs. 5(b), 5(d), and 5(f). It is clear that before current saturation [point (a) in Fig. 4], that even at the maximum e-beam defocus position (the anode plane) the electron density drops to zero before the vertical boundaries of the simulation space. This implies, because reflecting boundaries are assumed, that there is no interaction of the electron beams from adjacent emission sites 60 μm away. As the anode voltage is increased and the $J-V$ curve enters saturation [points (b) and (c) in Fig. 4], the electron density at the vertical boundaries starts to become significant [Figs. 5(b) and 5(d)]. This is indicative of beam interaction from neighboring emitters, and hence the onset of a space charge saturation. The increase in current density is now not sustained by higher velocity of the electrons arriving at the anode, but rather an increase in the density of electrons at the anode. This current saturation mechanism due to the interaction of emitting beams is a major advantage for vacuum power switches. It provides a mechanism of ''natural'' current limiting which is important for the short circuit safer operation of a power switch. It is interesting to note that in the saturated region the current density can be fitted by a $J=\mathrm{kV}^n$ relationship where $n=5/2$. Since this is also what is observed in experiment, it suggests that the saturation mechanism from multi-emitter FE cathode does not conform to the classical $J=\mathrm{kV}^{3/2}$ relationship used in single emitter thermionic cathodes.

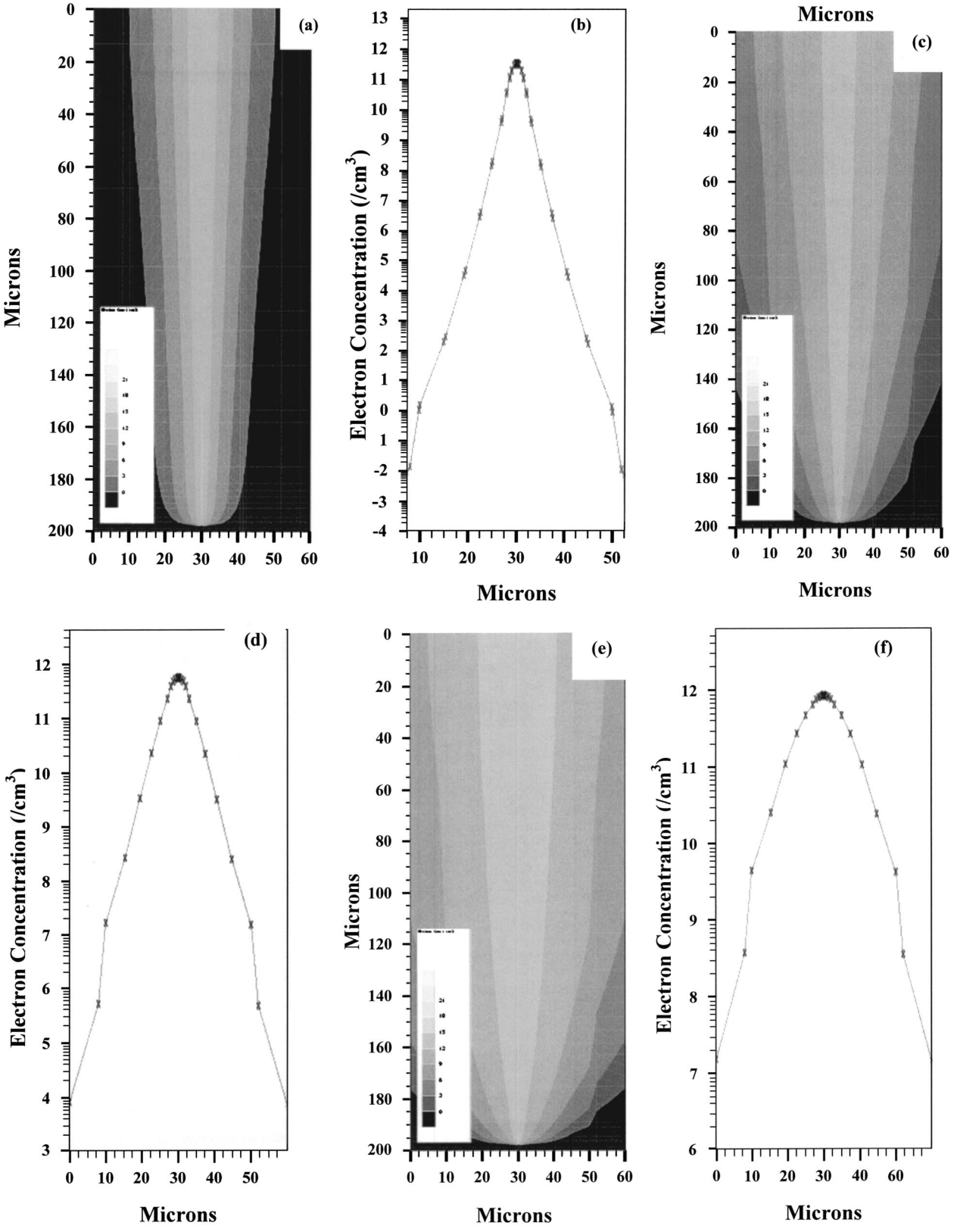

FIG. 5. Representation of the beam profile and electron density (a) and (b) before saturation (c) and (d) when emission starts to saturate and (e) and (f) after saturation.

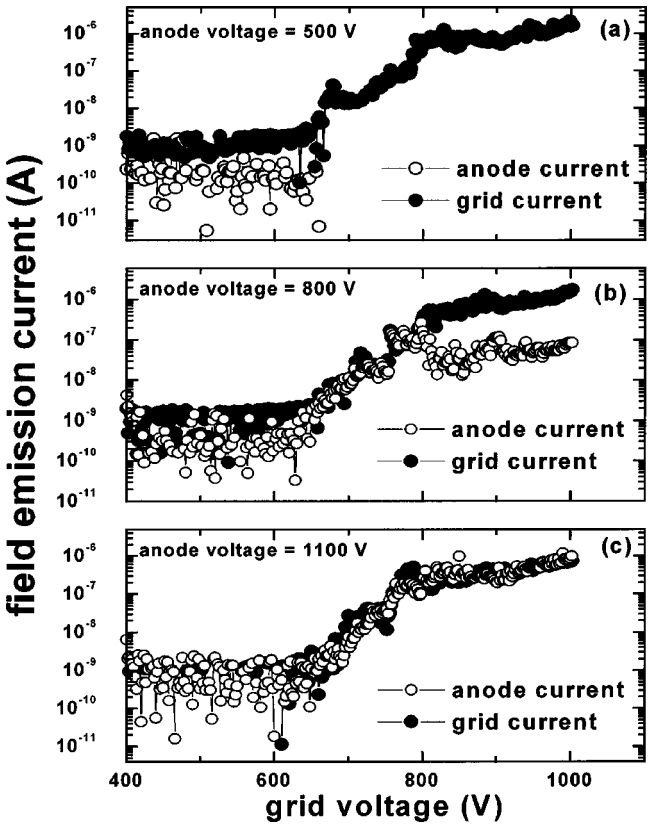

FIG. 6. Field emission characteristics of the triode structure as a function of the grid voltage (swept from 400 to 1100 V) and keeping the anode voltage constant at (a) 500 V, (b) 800 V, and (c) 1100 V.

Field emission characteristics from the triode structure experiment are shown in Fig. 6. A large grid-cathode separation (180 μm) was selected to avoid any contact with the nanotubes and to avoid a complicated device fabrication process. Since the turn on fields for this type of cathode were $\sim 2-3$ V/μm, this grid-cathode separation was enough to extract a reasonable amount of electrons. Anode cathode separation was kept at 1 mm. When the grid voltage was increased from 400 to 1100 V keeping the anode voltage constant at 500 V, no anode current was observed [Fig. 6(a)]. When the anode voltage was increased to 800 V some anode current ($\sim 0.1\ \mu$A) was measured [Fig. 6(b)]. The anode current was about one order of magnitude less than the grid current ($\sim 1\ \mu$A). The maximum anode current of $\sim 0.3\ \mu$A was measured at a grid voltage of around 800 V and a slight decrease in anode current was seen for grid voltages higher than the anode voltage. This is attributed to the negative potential gradient imposed by the grid so that only electrons with sufficient energy are able to reach the anode. Further increase in anode voltage to 1100 V showed an order of magnitude increase in anode current to $\sim 1\ \mu$A [Fig. 6(c)]. Although a small decrease in grid current with the increase in grid voltage was seen, the current gain was one. When no gate voltage was applied, the anode current was found to be below the noise level at the maximum applied anode voltage. Field emission characteristics of this simple triode structure show that at maximum only 50% of the emitted electrons are collected by the anode in this configuration. The grid current saturation for all anode voltage values occurred at $\sim 1\ \mu$A and 4.4 V/μm. However, it is difficult to calculate a current density due to the high transparency of the grid. Whereas when the anode voltage was 500 V, even the electrons with highest energy were unable to reach the anode. Further increase in anode voltage to 1100 V allowed more electrons to reach the anode at higher velocities, leading to an increase in the anode current. The saturation of the anode current seems to be due to the inability of additional electrons to pass through the grid. Otherwise the increase in grid voltage (lowering of anode-grid field) should result in a decrease of anode current. However, the grid field could also give the electrons a velocity parallel to the anode plane, causing the electron beam to spread. The simulation results confirm this and show that having a grid or a gate without some sort of a focusing grid allows the electron beam spread. Based on the simulation work performed by Lan *et al.* on gated Spindt tips, it is likely that a coaxial-type focusing structure will give the best result.[21] More simulation and experimental work is needed to focus and reduce the electron beam diameter to avoid losing current to the control grid in an optimized device.

IV. CONCLUSIONS

It is shown that the best field emission properties from carbon nanotube cathodes are obtained when their heights, diameters and spacings are optimized. Field emission currents as high as 10 mA have been obtained from 1 cm $\times$1 cm vertically aligned CNT cathodes with optimized parameters grown using dc plasma CVD *in situ*. The threshold field for the VACNT cathodes is typically 2 V/μm. Cathodes using carbon nanotubes with optimized electron emission characteristics were used to construct a vacuum power diode and three terminal triode devices. We have found that in order to obtain large emission current of >10 mA, space charge effects within the electron beam must be taken into account. The space charge forces cause the beam to spread radially. This beam spreading leads to interaction of the electrons emitted from different points on the cathode plane. This beam interaction leads to an effective current saturation mechanism in multi-emitter FE cathode devices. Reduction of the beam spreading has to be achieved in an optimum vacuum switch designed for blocking high voltage and having higher on current at low anode voltage.

[1]V. I. Merkulov, D. H. Lowndes, Y. Y. Wei, G. Eres, and E. Voelkl, Appl. Phys. Lett. **76**, 3555 (2000).
[2]A. C. Dillon, K. M. Jones, T. A. Bekkedahi, C. H. Kiang, D. S. Bethune, and M. J. Heben, Nature (London) **386**, 377 (1997).
[3]B. Gao, A. Kleinhammes, X. P. Tang, C. Bower, L. Fleming, Y. Wu, and O. Zhou, Chem. Phys. Lett. **307**, 153 (1999).
[4]C. M. Niu, E. K. Sichel, R. Hoch, D. Moy, and H. Tennent, Appl. Phys. Lett. **70**, 1480 (1997).
[5]J. N. Barisci, G. G. Wallace, and R. H. Baughman, J. Electroanal. Chem. **488**, 92 (2000).
[6]E. Frackwiak, K. Metenier, V. Bertagna, and F. Beguin, Appl. Phys. Lett. **77**, 2421 (2000).

[7]W. A. de Heer, A. Chatelaine, and D. Ugarte, Science **270**, 1179 (1995).
[8]J. M. Bonard, J. P. Salvetat, T. Stockli, L. Forro, and A. Chatelain, Appl. Phys. A: Mater. Sci. Process. **69**, 245 (1999).
[9]J. M. Kim, W. b. Choi, N. S. Lee, and J. E. Jung, Diamond Relat. Mater. **9**, 1184 (2000).
[10]W. Zhu, C. Bower, O. Zhou, G. Kochanski, and S. Jin, Appl. Phys. Lett. **75**, 873 (1999).
[11]P. G. Collins and A. Zettl, Appl. Phys. Lett. **69**, 1969 (1996).
[12]J.-M. Bonard, J. P. Salvetat, T. S. Ckli, W. A. de Heer, L. S. Forro, and A. C. Telain, Appl. Phys. Lett. **73**, 918 (1998).
[13]J.-M. Bonard, F. Maier, T. Stockli, A. Chatelain, W. A. de Heer, J. P. Salyetat, and L. Forro, Ultramicroscopy **73**, 7 (1998).
[14]K. A. Dean and B. R. Chalamala, Appl. Phys. Lett. **76**, 375 (2000).
[15]P. G. Collins and A. Zettl, Phys. Rev. B **55**, 9391 (1997).
[16]J.-M. Bonard, J. P. Salvetat, T. Stockli, L. S. Forro, and A. Chatelain, Appl. Phys. A: Mater. Sci. Process. **69**, 245 (1999).
[17]M. Chhowalla, K. B. K. Teo, C. Ducati, N. L. Rupesinghe, G. A. J. Amaratunga, A. C. Ferrari, D. Roy, J. Robertson, and W. I. Milne, J. Appl. Phys. **90**, 5308 (2001).
[18]SILVACO International.
[19]M. Chhowalla, C. Ducati, N. L. Rupesinghe, K. B. K. Teo, and G. A. J. Amaratunga, Appl. Phys. Lett. **79**, 2079 (2001).
[20]S. B. Lee, K. B. K. Teo, L. A. W. Robinson, A. S. Teh, M. Chhowalla, D. G. Hasko, G. A. J. Amaratunga, W. I. Milne, and H. Ahmed, Proceedings of the 46th International Conference on Electron, Ion and Photon Beam Technology and Nanofabrication, Anaheim, CA, 2002.
[21]Y. C. Lan, J. T. Lai, S. H. Chen, W. C. Wang, C. H. Tsai, and C. Y. Sheu, J. Vac. Sci. Technol. B **18**, 911 (2000).